Microscopic origin of chiral shape induction in achiral crystals

Wende Xiao[1,2], Karl-Heinz Ernst[1,3], Krisztian Palotas[4], Yuyang Zhang[2], Emilie Bruyer[5], Lingqing Peng[6], Thomas Greber[7], Werner A. Hofer[8], Lawrence T. Scott[6], & Roman Fasel[1,9*]

[1] Empa, Swiss Federal Laboratories for Materials Science and Technology, Überlandstrasse 129, 8600 Dübendorf, Switzerland.

[2] Institute of Physics, Chinese Academy of Sciences, 100190 Beijing, China

[3] Department of Chemistry, University Zürich, Zürich, Switzerland

[4] Department of Theoretical Physics, Budapest University of Technology and Economics, Hungary

[5] CNR-SPIN, I-67010, L'Aquila, Italy

[6] Department of Chemistry, Merkert Chemistry Center, Boston College, Chestnut Hill, MA 02467-3860, USA

[7] Department of Physics, University Zürich, Zürich, Switzerland

[8] School of Chemistry, Newcastle University, Newcastle, UK

[9] Department of Chemistry and Biochemistry, Universität Bern, Bern, Switzerland

[*] email: roman.fasel@empa.ch

In biomineralisation, inorganic materials are formed with remarkable control of shape and morphology. Chirality, as present in the biomolecular world, is therefore also common for biominerals. Bio-macromolecules, like proteins and polysaccharides are in direct contact with the mineral phase and act as modifiers during nucleation and crystal growth. Due to their homochirality – they exist only as one of two possible mirror symmetric isomers – their handedness is often transferred into the macroscopic shape of the biomineral crystals, but yet the way in which handedness is transmitted into achiral materials is not understood at the atomic level. By using the submolecular resolution capability of scanning tunnelling microscopy, we show how the chiral 'buckybowl' hemibuckminsterfullerene arranges copper surface atoms in its vicinity into a chiral morphology. We anticipate that such new insight will find its way into materials synthesis techniques.

Influencing the macroscopic shape of a crystal during growth requires molecular tectonics, i.e., adsorbed molecules that arrange and stabilize new sites at the surface of the material[1].

Today, crystallization at the crystal/liquid interface can be investigated at high resolution with scanning probe microscopy, but so far such studies have addressed only the growth of the mineral phase itself[2,3]. Previous investigations have addressed the reorganization of inorganic surfaces by achiral and chiral molecules[4-7]. However, the microscopic role that molecules play during crystal growth, for example as surfactants at step edges, remains poorly understood[8,9]. All steps of crystal growth, including adsorption of atoms or molecules from the liquid or gas phase onto the crystal surface, migration across the surface and along step edges, incorporation at kink or step sites, and nucleation of new islands, are also available at the metal–vacuum interface. This opens a way to study molecular tectonics and crystal growth with the high precision provided by scanning tunnelling microscopy (STM)[10]. The Cu(110) surface, with its high mobility of top-layer atoms at room temperature[11], provides an excellent model system for studying initial steps of crystal shaping by molecules. In order to significantly influence the morphology of the crystal, the organic modifier needs to interact sufficiently with the inorganic material. For the most abundant biomineral calcite, for example, dicarboxylic acids have been identified as efficient modifiers, because both carboxylate groups interact strongly with calcium ions[12].

In the case of copper, polar molecules like carboxylic acids, amino acids and chiral ketones have been identified as suitable chiral modifiers for induction of handed shape into the crystal surface[6,13-18]. However, as the binding configurations of the molecules at the kink sites were poorly resolved, a microscopic picture of chiral recognition and chiral crystal surface formation has not been obtained so far. Here we show that the aromatic chiral buckybowl hemifullerene ($C_{30}H_{12}$, Fig. 1a), basically representing half of a C_{60} buckyball and lacking any functional groups, can also act as a crystal shape modifier. We find that certain chiral kinks are stabilized by metal-organic coordination bonds, whereby opposite mirror isomers, so-called enantiomers, create opposite chiral kinks. In our work, the absolute handedness of the molecules is obtained with submolecular resolution STM in combination with synchrotron radiation X-ray photoelectron diffraction (XPD), disclosing the orientation of the bowl at the chiral kink sites. The exact binding geometry of the chiral buckybowl at the kink is identified via density functional theory (DFT), which reveals that the chiral recognition of hemifullerene at the Cu(110) surface can be explained with the classical three point contact model.

Results and discussion

After deposition of ~15% of a close-packed monolayer of the racemic (1:1) mixture of *M*- and *P*-enantiomers[19] at room temperature (RT) and cooling to 50 K, the Cu surface shows remarkable signs of restructuring. Step edges exhibit a pronounced saw-tooth shape with straight segments parallel to the $[\bar{3}3\bar{4}]$ and $[\bar{3}34]$ directions of the surface plane (Fig. 1b). In addition, islands with an asymmetric shape are formed on the terraces, with their edges also aligned along the $[\bar{3}3\bar{4}]$ and $[\bar{3}34]$ directions (Fig. 1c). Each of these directions breaks the mirror symmetry of the underlying Cu(110) surface, and all step edges are decorated with hemifullerene molecules. Single hemifullerene molecules on the flat terraces are only observed at low temperatures (Fig. 1b), because they are too mobile at room temperature to be imaged by STM (Fig. 1c).

The asymmetric shape of the islands and the mirror symmetry breaking direction of the step edges suggest an enantioselective decoration. That is, $[\bar{3}3\bar{4}]$ steps are decorated with one type of enantiomer and the $[\bar{3}34]$ steps with the other. The equal STM appearance of molecules at the same type of step indeed supports this conclusion. Very narrow elongated islands are also observed, which are decorated with one enantiomer only (Fig. 2 a,c,d). Considering the C_3-symmetry of the hemifullerene molecules, it is not possible to assign the absolute handedness solely from STM. If the C_3 axis of the molecular bowl were normal to the surface, then the three uppermost C6 rings would be at identical height above the surface and, hence, it would be impossible to determine the intrinsic handedness of a hemifullerene molecule via STM. However, all molecules show a pronounced contrast in STM due to a tilted adsorption geometry. With the knowledge of the exact adsorption geometry, it becomes therefore possible to conclude on the handedness from STM. Detailed conclusions on the orientation of the molecules on the surface is achieved here with XPD[20]. Because XPD is an averaging technique for a larger surface area, both surface species – terrace and step edge molecules – as well as their relative abundance need to be taken into account. Using the ratio of step and terrace molecules at a given coverage – obtained by counting the molecules in large-scale STM images – the best fit to the XPD pattern was obtained with a tilt of the molecular C_3 axis away from the surface normal by 10° at the terrace and 18° at the step edge (Supplementary Figures 1-3; for details on the XPD data analysis see the Supplementary Information).

With the knowledge of the adsorbate geometry, in particular the polar tilt angle and the tilt direction of the molecular bowl, the STM appearance has been modelled and compared to the experimental results (Fig. 2). As previously observed for the buckybowl corannulene[21,22], hemifullerene interacts with its convex side with the Cu surface. On flat terraces, three bright lobes in the STM appearance of a single molecule coincide with the three outer C6 rings (Fig. 2e-g). They are imaged at different intensity, reflecting that the molecule is slightly tilted by 10° (Fig. 2h). This fact allows the determination of the molecular handedness by modelling the STM appearance for a given tilt of the C_3 axis of the bowl (Fig. 2g). A clockwise height decrease of the three C6 rings identifies an *M*-enantiomer (Fig. 2g), whereas a counterclockwise height decrease is assigned to the *P*-enantiomer (see Supplementary Figure 1). However, the adsorption geometry at the step edge differs substantially from the one on the terraces. Because of the larger tilt of the molecular bowl of 18° along a different direction (see Supplementary Figure 1), the height-decrease sequence of the three outer C6 rings turns into the opposite sense for the same enantiomer on the step edge with respect to the situation on the flat terrace. The *M*-enantiomer shows for example a clockwise contrast sequence on the terrace (Fig. 2e-h), but a counterclockwise contrast sequence at the step edge (Fig. 2i-l). For correct assignment of the contrast sequence of molecules that are not isolated, e.g., molecules decorating a step edge in a single line, we started the analysis at the end of the line (corner molecule), in order to make sure that only lobes from the same single molecule were evaluated. Altogether, such detailed contrast analysis of this complex situation reveals that step edges running parallel to the $[\bar{3}3\bar{4}]$ direction are exclusively decorated with *M*-enantiomers and step edges running parallel to the $[\bar{3}34]$ direction are decorated only with *P*-enantiomers (for details see Supplementary Figure 4).

Molecular and stereoselective recognition at crystal surfaces has been known for some time[23-25], and that enantiomers bind preferentially to chiral kinks has been shown before[26-31]. By contrast, here the chiral kinks are created by a chiral molecule. A step edge running along the $[\bar{3}3\bar{4}]$ direction has chiral *R*-kinks; the one running along the $[\bar{3}34]$ direction has *S*-kinks (Fig. 3). With a kink periodicity of 1.053 nm they basically span over two closed-packed Cu rows of this (110) surface. For stepped and kinked face centred cubic (fcc) crystal surfaces, special notations have been proposed[32]. The *R/S* denominators for the handedness of kinks are based on the clockwise or counter clockwise sequence of (100), (110), and (111)

facets at the kink, involving a lower terrace facet (Supplementary Figure 5)[26]. From this it follows that *M*-hemifullerene creates *R*-kinks and *P*-hemifullerene *S*-kinks.

In order to understand how the molecule creates a chiral kink, the exact bonding situation at the kink has been evaluated with DFT calculations. The most stable adsorption configurations of *M*-enantiomers at the *R*- and *S*-kinks have been searched by simulated annealing molecular dynamics calculations (see Methods for details). After geometrical optimization, the *M*-enantiomer at the *R*-kink site is indeed found to be the most favourable configuration (for a comparison of the configurations determined from DFT and from the XPD analysis, see Supplementary Figure 6). Or in other words, *M*-hemifullerene can only stabilize an *R*-kink Cu atom at the upper step because of such bonding configuration. With a total binding energy of 4.66 eV, the adsorbate is stabilized by 0.14 eV over the lowest energy configuration of an *M*-hemifullerene located at an *S*-kink site (see Supplementary Figure 7), and by 0.5 eV over a *M*-hemifullerene at a straight step edge (see Supplementary Figure 8). This energy difference is at the upper level of previously reported values of enantioselectivity (0.01 to 0.14 eV) for chiral kink adsorption,[28-31] whereby the largest experimental values do not exceed 0.04 eV.[33,34]

The nature of the chemical bonding has been evaluated via charge density difference distribution analysis (Fig. 4 d-f). It reveals that chiral kink creation is driven by three η^1-coordinated Cu-C bond, i.e., a single bond is formed between a Cu surface atom and a carbon atom, and three η^2-coordinated Cu-C bonds, i.e., each bond goes from a single Cu atom to two adjacent carbon atoms of the molecule (Fig. 4, Supplementary Figure 9). The six carbon atoms involved in the three η^2 bonds are all located in the central C6 ring of the hemifullerene, from which one of the η^2 bonds goes to the kink atom. The two other η^2 bonds go to adjacent Cu atoms on the lower terrace. A similar two-Cu-atom binding site in the lower terrace establishes two η^1 bonds to C-atoms in the same C5 ring (labeled 2 & 3 in Supplementary Figure 9a), while the remaining η^1 bond goes to a step edge atom next to the kink atom. All bond lengths are between 2.11 Å and 2.27 Å. The four Cu atoms of the binding site on the lower terrace represent a single (110) surface unit cell. When viewed from above, going from this terrace site via the step binding site to the kink atom is performed in a clockwise fashion for the *M*-hemifullerene/*R*-kink complex, but in a counterclockwise fashion in the case of the *P*-hemifullerene/*S*-kink complex. Hence, these three mirror-like binding sites involved in the chiral recognition of hemifullerene at the Cu(110) surface are a manifestation of the classical three point contact model of chiral

recognition.[35] The relatively strong Cu metal-fullerene interaction leads to the effect that at room temperature diffusing Cu atoms are captured by the hemifullerene molecules and the surface becomes restructured in the observed manner. This also leads to the formation of homochiral hemifullerene stabilized adatom wires. Adsorption of only one enantiomer would lead to single-handed structures and to stabilisation of only one type of nanowire or handed material. For the particular case of hemifullerene, however, all attempts to separate the enantiomers were unfortunately unsuccessful so far.

Conclusions

In conclusion, we have shown under abiotic conditions and using submolecular-resolution STM, XPD and DFT calculations that the chiral geodesic hydrocarbon hemibuckminsterfullerene restructures a metal surface in such a way that chirality is imprinted onto the metal. Such a restructuring can be considered as the first step towards the modification of achiral crystals into a chiral shape. At the microscopic level, chiral recognition occurs here via metal-organic coordination bonding between copper atoms near step edges and specific molecular binding sites. Mobile Cu adatoms are immobilized into homochiral nanowires or chiral islands. Although a special example of restructuring of a crystal (aromatic molecule and apolar metal), our example here involves the elementary processes, such as formation of kinks and chiral recognition at surfaces, that are of paramount importance for shape induction in biomineralisation. Beyond step edge propagation and step edge morphology, which were previously studied for biominerals with scanning probe microscopy, our work now also reveals detailed insight into the interplay between the molecular modifier and the inorganic mineral phase.

Methods

Hemifullerene was synthesized according to the method of Scott *et al.*[36]. Experiments were carried out in two independent ultrahigh vacuum (UHV) systems. The variable-temperature STM system (Omicron Nanotechnology) is equipped with low-energy electron diffraction (LEED) and standard surface preparation facilities. The Cu(110) single-crystal was prepared by repeated cycles of sputtering with argon ions (typically at an argon pressure of 2×10^{-5} mbar and an acceleration voltage of 1.5 kV) and annealing at ~ 700 K. Before deposition of hemifullerene, cleanliness and surface order were checked by LEED and STM. Hemifullerene was sublimated from a Knudsen-cell type evaporator at a temperature of 480

K, while the Cu(110) substrate was held at room temperature. STM images were acquired in constant-current mode either at room temperature or at a sample temperature of ~ 50 K. The XPD experiments were performed at the NearNode endstation of the Surface and Interface Microscopy Beamline of the Swiss Light Source using linearly polarized synchrotron X-ray radiation of 920 eV. The C 1s (E_{kin} = 626 eV) XPD patterns were collected with the sample held at room temperature. Single scattering cluster (SSC) simulations were used to find the molecular orientation yielding the lowest reliability factor (*R* factor) and hence the best agreement with experiment[37,38]. Backscattering from substrate atoms was neglected since the backscattering yield is very low within the kinetic-energy range used for this work (>400 eV).

DFT calculations were performed using the Vienna ab initio simulation package (VASP)[39] in a generalized gradient approximation (GGA)[40]. The projector augmented wave (PAW) method was employed[41]. The van der Waals (vdW) interactions were described by the method of Tkatchenko and Scheffler (DFT-TS)[42], which significantly improves the accuracy for aromatic molecules on metal substrates[43]. The periodic slab models include four Cu layers, a kinked step, the *M*-enantiomer of hemifullerence (a total of 161 atoms), and a vacuum layer larger than 19 Å. The most stable adsorption configurations of *M*-hemifullerene at different kinked steps were searched by the simulated annealing method[44] based on molecular dynamics calculations[45], which is widely used in structure prediction without requiring reasonable structual inputs but relying on temperature evolution in time[46,47]. The annealing starts with configurations far from equilibrium. The systems were then cooled down from 300 K to 0 K in 9 ps with 2 fs time steps and further relaxed at 0 K. The slow annealing process allows the molecule to cover a sufficiently large phase space and to find the most stable adsorption configuration. In the optimization process, the bottom three Cu layers were frozen. The surface Cu layer, the kinked step edge atoms and the molecule were fully relaxed until the residual forces were smaller than 0.015 eV/Å. A 400 eV energy cutoff for the plane-wave basis sets and Γ-point k-sampling in reciprocal space were used.

References

1. Mann, S. Molecular tectonics in biomineralization and biomimetic materials chemistry. *Nature* **365**, 499-505 (1993).

2. Orme, C. A. *et al.* Formation of chiral morphologies through selective binding of amino acids to calcite surface steps. *Nature* **411**, 775-779 (2001)

3. Qiu, S. R. *et al.* Modulation of calcium oxalate monohydrate crystallization by citrate through selective binding to atomic steps. *J. Am. Chem. Soc.* **127**, 9036-9044 (2005).

4. Switzer, J. A., Kothari, H. M. Poizot, P., Nakanishi, S. & Bohannan, E. W. Enantiospecific electrodeposition of a chiral catalysts, *Nature* **425**, 490-493 (2003).

5. Schaaff, T. G. & Whetten, R. L. Giant gold-glutathione cluster compounds: Intense optical activity in metal-based transitions. *J. Phys. Chem. B* **104***,* 2630-2641 (2000).

6. Zhao, X. Fabricating homochiral facets on Cu(001) with L-lysine. *J. Am. Chem. Soc.* **122**, 12584-12585 (2000).

7. Abadía, M. *et al.* Massive surface reshaping mediated by metal−organic complexes, *J. Phys. Chem. C* **118**, 29704−29712 (2014).

8. Addadi, L. & Weiner, S. Crystals, Asymmetry and life, *Nature* **411**, 753-755 (2001).

9. Bouropoulos, N., Weiner, S. & Addadi, L. Calcium oxalate crystals in tomato and tobacco plants: morphology and in vitro interactions of crystal-associated macromolecules, *Chem. Eur. J.* **7**, 1881-1888 (2001).

10. Chen, Q. & Richardson, N. V. Surface faceting induced by adsorbates. *Prog. Surf. Sci.* **73**, 59-77 (2003).

11. Coulman, D. J., Wintterlin, J., Behm, R. J. & Ertl, G. Novel mechanism for the formation of chemisorption phases: The (2× 1) O-Cu (110)‘‘added row’’ reconstruction. *Phys. Rev. Lett.* **64,** 1761-1764 (1990).

12. Mann, S., Didymus, J. M., Sanderson, N. P., Heywood, B. R. & Samper, E. J. A. Morphological influence of functionalized and non-functionalized D-alpha, omega-dicarboxylates on calcite crystallization. *J. Chem. Soc., Faraday Trans.* **86**, 1873-1880 (1990).

13. Mhatre, B. *et al.* A window on surface explosions: tartaric acid on Cu(110). *J. Phys. Chem. C* **117**, 7577-7588 (2013).

14. Schunack, M., Lægsgaard, E., Stensgaard, I., Johannsen, I., & Besenbacher, F. A chiral metal surface. *Angew. Chem. Int. Ed.* **40**, 2623-2626 (2001).

15. Karageorgaki, C. & Ernst, K.-H. A metal surface with chiral memory. *Chem. Commun. (Camb.)* **50,** 1814 (2014).
16. Karageorgaki, C., Passerone, D. & Ernst, K.-H. Chiral reconstruction of Cu(110) after adsorption of fumaric acid *Surf. Sci.* **629,** 75-80 (2014).
17. Roth, C., Parschau, M. & Ernst, K.-H. Chiral reconstruction of a metal surface by adsorption of racemic malic acid. *ChemPhysChem.* **12**, 1572-1577 (2011).
18. Zhao, X., Perry, S. S., Horvath, J. D. & Gellman, A. J. Adsorbate induced kink formation in straight step edges on Cu(533) and Cu(221). *Surf. Sci.* **563**, 217-224 (2004).
19. Petrukhina, M. A., Andreini, K. W., Peng, L. & Scott, L. T. Hemibuckminsterfullerene $C_{30}H_{12}$: X-ray crystal structures of the parent hydrocarbon and of the two-dimensional organometallic network $\{[Rh_2(O_2CCF_3)_4]_3 \cdot (C_{30}H_{12})\}$. *Angew. Chem. Int. Ed.* **43**, 5477-5481 (2004).
20. Fasel, R. & Aebi, P. X-ray photoelectron diffraction: Probing atom positions and molecular orientation at surfaces. *Chimia* **56**, 566-572 (2002).
21. Parschau, M. *et al.* Buckybowls on metal surfaces: Symmetry mismatch and enantiomorphism of corannulene on Cu(110). *Angew. Chem. Int. Ed.*, **46** 8258-8261 (2007)
22. Merz, L. *et al.* Reversible phase transitions in a buckybowl monolayer. *Angew. Chem. Int. Ed.* **48**, 1966–1969 (2009).
23. Weissbuch, I., Addadi, L., Lahav, M. & Leiserowitz, L. Molecular recognition at crystal surfaces, *Science* **253**, 637-645 (1991).
24. Hazen, R. M. & D. S. Sholl, D. S. Chiral selection on inorganic crystalline surfaces. *Nature Mater.* **2**, 367-374 (2003).
25. Hazen, R. M., Filley, T. R. & Goodfriend, G. A. Selective adsorption of L- and D amino acids on calcite: Implications for biochemical homochirality. *Proc. Natl. Acad. Sci. USA* **98,** 5487-5490 (2001).
26. Ahmadi, A., Attard, G., Feliu, J. & Rodes A. Surface reactivity at chiral platinum surfaces. *Langmuir* **15**, 2420-2424 (1999).

27. Ernst, K.-H. Molecular chirality at surfaces. *Phys. Status Solidi B* **249**, 2057-2088 (2012).

28. Kühnle, A., Linderoth, T. R. & Besenbacher, F. Enantiospecific adsorption of cysteine at chiral kink sites on Au(110)-(1×2). *J. Am. Chem. Soc.* **128**, 1076-1077 (2006).

29. Greber, T., Šljivančanin, Ž., Schillinger, R., Wider, J. & Hammer, B. Chiral recognition of organic molecules by atomic kinks on surfaces. *Phys. Rev. Lett.* **96**, 56103-56106 (2006).

30. Rankin, R. B. & Sholl, D. S. First-principles studies of chiral step reconstructions of Cu(100) by adsorbed glycine and alanine. *J. Chem. Phys.* **124**, 074703/1-6 (2006).

31. Cheong, W. Y. & Gellman, A. J. Energetics of chiral imprinting of Cu(100) by lysine. *J. Phys. Chem. C* **115***,* 1031-1035 (2011).

32. Van Hove, M. A. & Somorjai, G. A. A new microfacet notation for high-Miller-index surfaces of cubic materials with terrace, step and kink structures. *Surf. Sci.* **92**, 489-518 (1980).

33. Yun, Y. & Gellman, A. J. Enantioselective Separation on Naturally Chiral Metal Surfaces: D,L-Aspartic Acid on Cu(3,1,17) R&S Surfaces. *Angew. Chem. Int. Ed.* **52**, 3394–3397 (2013).

34. Fleming, C.; King, M. & Kadodwala, M. Highly Efficient Electron Beam Induced Enantioselective Surface Chemistry. *J. Phys. Chem. C* **112**, 18299−18302 (2008).

35. Easson, L. H. & Stedman, E. Studies on the relationship between chemical constitution and physiological action. *Biochem.* **27**, 1257-1266 (1933).

36. Hagen, S., Bratcher, M. S., Erickson, M. S., Zimmermann, G. & Scott, L. T. Novel syntheses of three $C_{30}H_{12}$ bowl-shaped polycyclic aromatic hydrocarbons. *Angew. Chem. Int. Ed.* **36**, 406-408 (1997).

37. Fadley, C. S. The study of surface structures by photoelectron diffraction and Auger electron diffraction, in Synchrotron Radiation Research: Advances in Surface Science, edited by R. Z. Bachrach (Plenum, New York, 1992), p. 421.

38. Fasel, R., *et al.* Local structure of *c*(2×2)-Na on Al(001): Experimental evidence for the coexistence of intermixing and on-surface adsorption, *Phys. Rev. B* **50**, 14516-14524 (1994).

39. Kresse, G. & Furthmüller, J. Efficient iterative schemes for ab initio total-energy calculations using a plane-wave basis set. *Phys. Rev. B* **54**, 11169-11186 (1996).
40. Perdew, J. P., Burke, K. & Ernzerhof, M. Generalized gradient approximation made simple, *Phys. Rev. Lett.* **77**, 3865-3868 (1996).
41. Blöchl, P. E., Projector augmented-wave method, *Phys. Rev. B* **50**, 17953-17979 (1994).
42. Tkatchenko, A. & Scheffler, M. Accurate molecular van der Waals interactions from ground-state electron density and free-atom reference data, *Phys. Rev. Lett.* **102**, 073005 (2009).
43. Lüder, J., Sanyal, B., Eriksson, O., Puglia, C. & Brena, B. Comparison of van der Waals corrected and sparse-matter density functionals for the metal-free phthalocyanine/gold interface, *Phys. Rev. B* **89**, 045416 (2014).
44. Kirkpatrick S., Gelatt Jr., C. D. & Vecchi, M.P., Optimization by simulated annealing, *Science* **220**, 671-680 (1983).
45. Car, R. & Parrinello, M. Unified approach for molecular dynamics and density-functional theory, *Phys. Rev. Lett.* **55**, 2471-2474 (1985).
46. Kresse, G. & Hafner, J. First-principles study of the adsorption of atomic H on Ni (111), (100) and (110), *Surf. Sci.* **459**, 287-302 (2000).
47. Cui., P. *et al.* Multipoint interactions enhanced CO_2 uptake: a zeolite-like zinc–tetrazole framework with 24-nuclear zinc cages *J. Am. Chem. Soc.* **134**, 18892 (2012).

Acknowledgements

Financial support from the Swiss National Science Foundation, the National Natural Science Foundation of China (61574170), the U.S. National Science Foundation, and the U.S. Department of Energy is gratefully acknowledged. K.P. and W.H. acknowledge EPSRC support for the UKCP consortium (grant reference EP/K013610/1). K.P. acknowledges the Hungarian Eötvös Fellowship. W.H. acknowledges support by the Royal Society London. R.F. thanks André Müller, Carlo A. Pignedoli and Oliver Gröning for the implementation of the multipole expansion algorithms used for the XPD-SSC analysis. We thank A. Tkatchenko

for fruitful discussions. The XPD experiments were performed on the SIM beamline at the Swiss Light Source, Paul Scherrer Institut, Villigen, Switzerland.

Author contributions

R.F. & K.H.E. perceived the experiments. W.X., T.G. & R.F. performed the experiments and data analysis. K.P., Y.Z., E.B. & W.H. conducted the theoretical modelling. L. P. & L.T.S. conducted the chemical synthesis. W.X., K.H.E. and R.F. wrote the manuscript with contributions from all authors.

Additional information

Supplementary information and chemical compound information are available in the online version of the paper. Reprints and permissions information is available online at www.nature.com/reprints. Correspondence and requests for materials should be addressed to R.F..

Competing financial interests

The authors declare no competing financial interests.

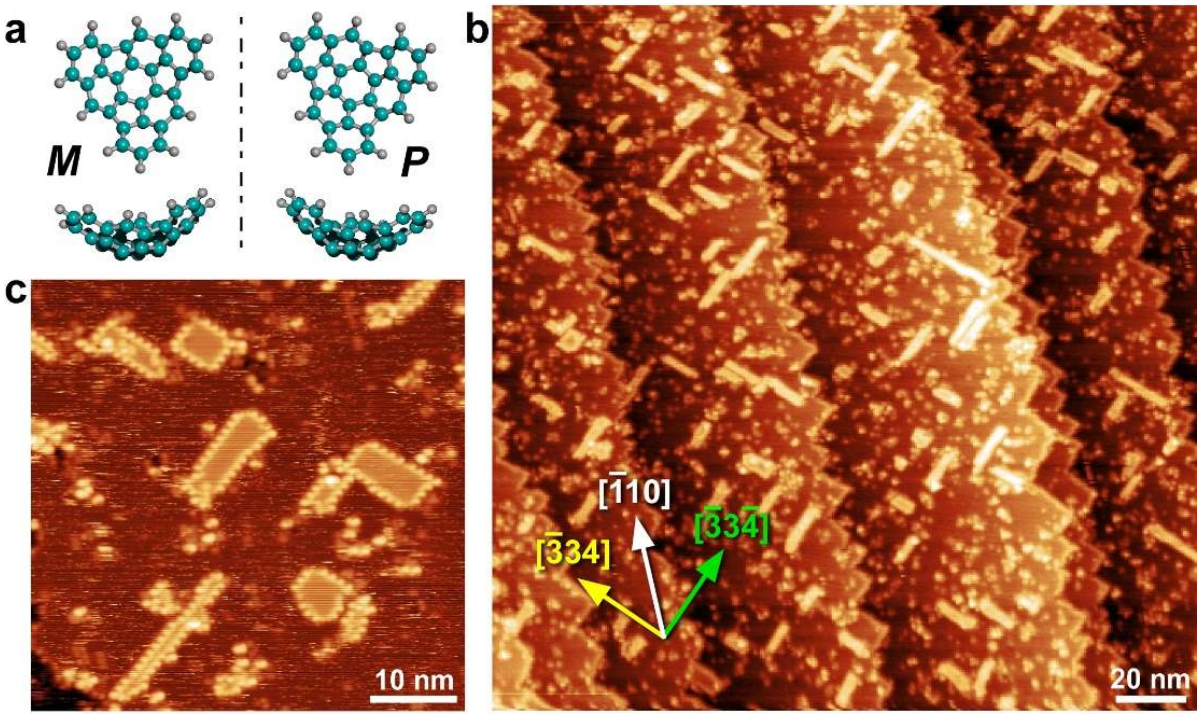

Figure 1 | Initial steps of chiral faceting of Cu(110) by hemifullerene. (**a**) Ball-and-stick models of *M*- and *P*-hemifullerene ($C_{30}H_{12}$), looking towards their concave side. (**b**) STM image (U = –2.0 V; I = 22 pA, T = 50 K) acquired after deposition of 15% of a complete monolayer of hemifullerene at room temperature. Instead of linear step edges along [$\bar{1}$10], as observed for clean Cu(110), the step edges are decorated with molecules and have a zigzag shape, exhibiting [$\bar{3}3\bar{4}$] and [$\bar{3}$34] directions. On the (110) terraces single molecules, nanowires and elongated islands with edges aligned along the [$\bar{3}3\bar{4}$] and [$\bar{3}$34] directions are observed. (**c**) STM image (U = –2.0 V; I = 23 pA, T = 300 K) of a step-free surface region acquired at room temperature. Decorated 2D islands are still observed on the terrace, with straight edges also running parallel to [$\bar{3}3\bar{4}$] and [$\bar{3}$34] directions. Single molecules are not observed between the decorated islands, but streaky features indicate diffusing molecules.

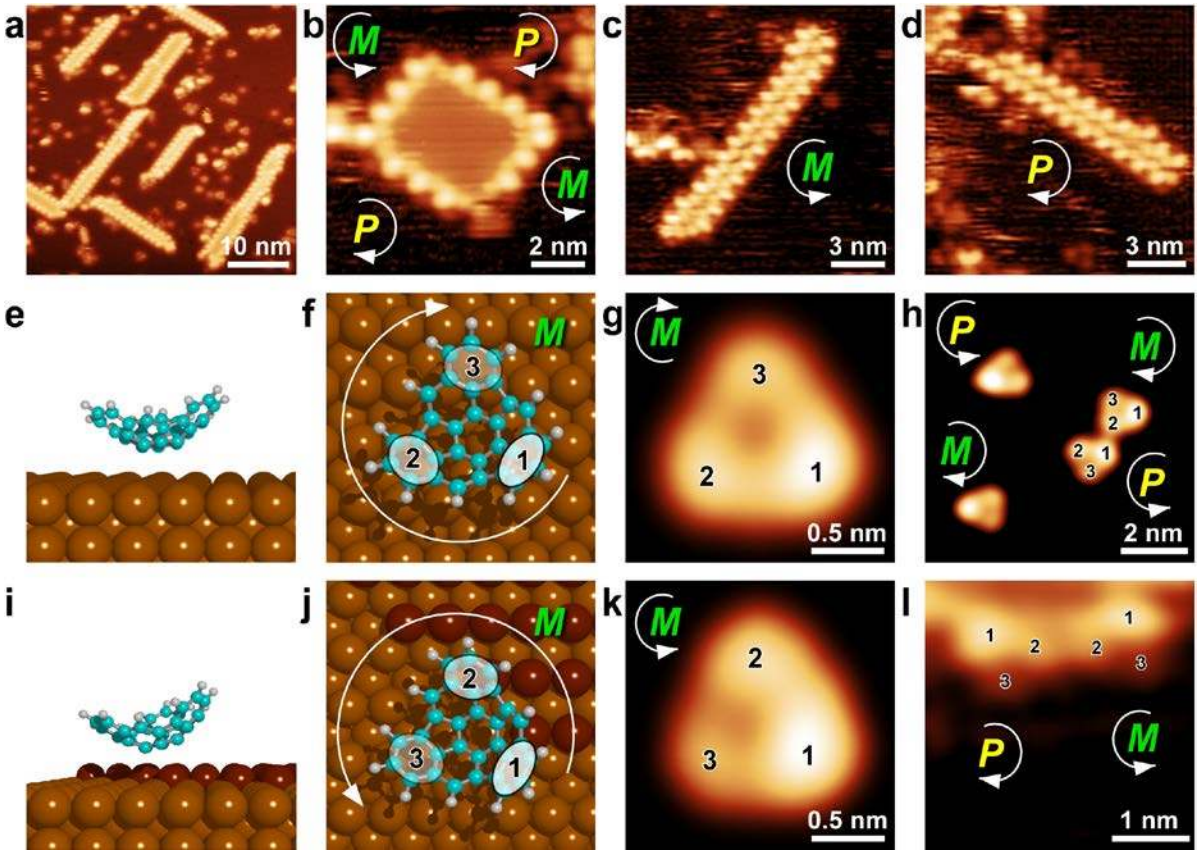

Figure 2 | Determination of the absolute handedness of hemifullerene molecules. (**a**) STM image showing elongated islands decorated with hemifullerene molecules and single hemifullerene molecules on the flat terrace (T= 50 K, U = –2.3 V; I = 23 pA). (**b-d**) Enantioselective step decoration of 2D Cu islands and Cu metal wires. Steps and wires running parallel to the $[\bar{3}3\bar{4}]$ direction are decorated with *M*-enantiomers, those running parallel to the $[\bar{3}34]$ direction are decorated with *P*-enantiomers (T = 300 K, U = –2.0 V; I = 23 pA for image b, U = –2.4 V; I = 35 pA for images **c**,**d**). (**e**,**f**) Side and top views of the best-fit molecular orientation of *M*-hemifullerene on the terrace, as obtained from XPD. The molecular C_3 axis is inclined by 10° with respect to the surface normal. The heights of the C6-rings above the surface plane are marked as highest (1), middle (2) and lowest (3), which gives rise to the different intensities of the three protrusions observed in STM images. (**g**) Simulation of STM appearance for a molecule on the flat terrace. In connection with the

knowledge of the tilt angle the absolute handedness is determined from the sequence of intensity (highest to lowest) of the three lobes. (**h**) STM image showing individual hemifullerene molecules on a flat Cu(110) terrace, and the assignment of their handedness (T= 50 K, U = –2.32 V, I = 30 pA). (**i**,**j**) Side and top views of the molecular orientation of *M*-hemifullerene at a step edge, as obtained from XPD. The molecular C_3 axis is inclined by 18° with respect to the surface normal. (**k**,**l**) Simulation of STM appearance of an *M*-enantiomer located at a step edge and an STM image (U = –2.2 V; I = 23 pA) showing both enantiomers at a corner of a 2D island.

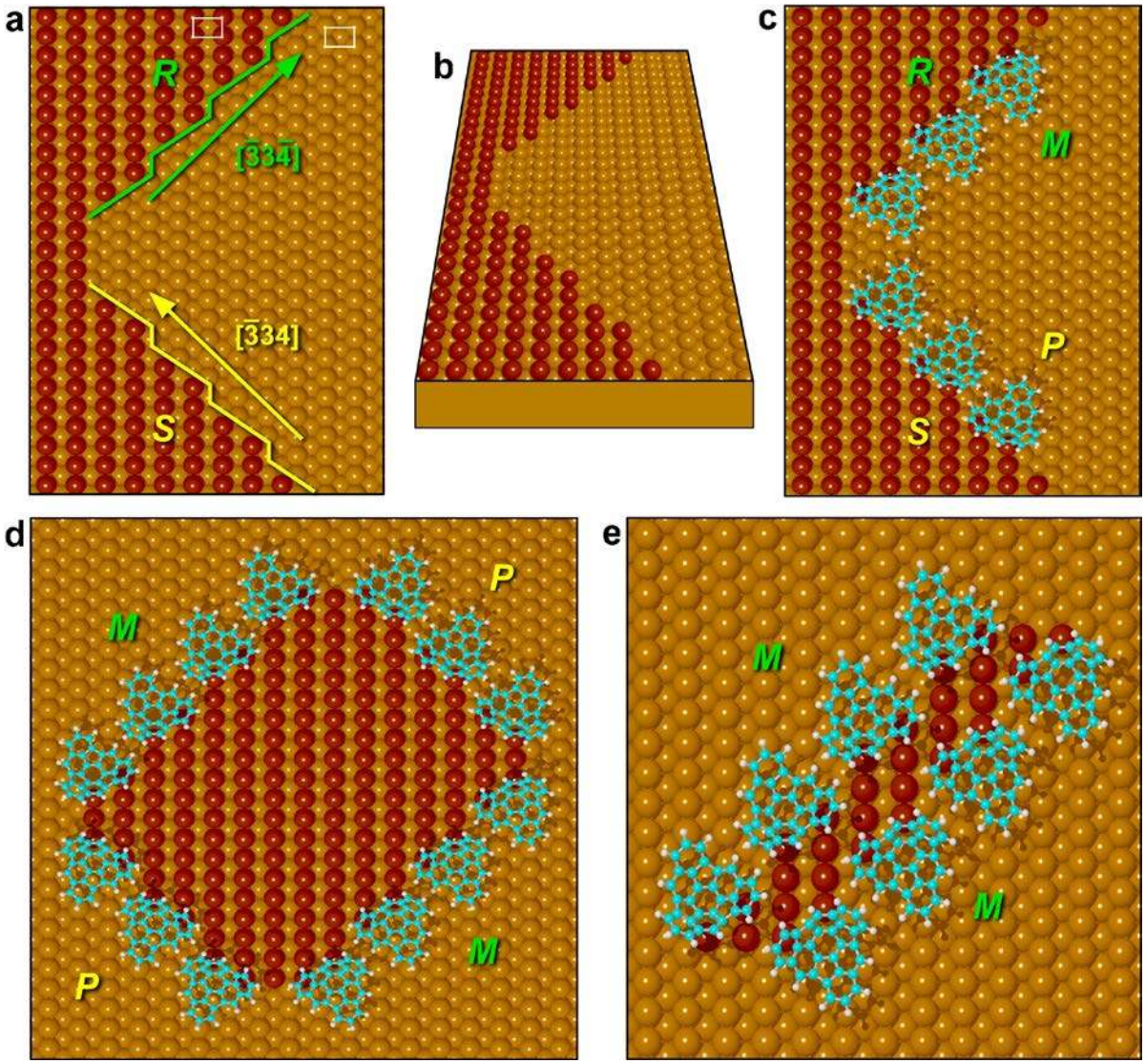

Figure 3 | Structure models for homochiral step edges. (**a**) Hard-sphere model of the observed step edge with alternating [$\bar{3}3\bar{4}$] and [$\bar{3}34$] segments and the formation of chiral kink sites. (**b**) Structure model of the observed steps along [$\bar{3}3\bar{4}$] and [$\bar{3}34$] with hemifullerene decoration. *M*-enantiomers decorate *R*-kinks, *P*-enantiomers decorate *S*-kinks. (**c**) Structural model of an adatom island stabilized by *M*- and *P*-hemifullerene. (**d**) Structural model of an *M*-hemifullerene stabilized Cu adatom nanowire running along the [$\bar{3}3\bar{4}$] direction.

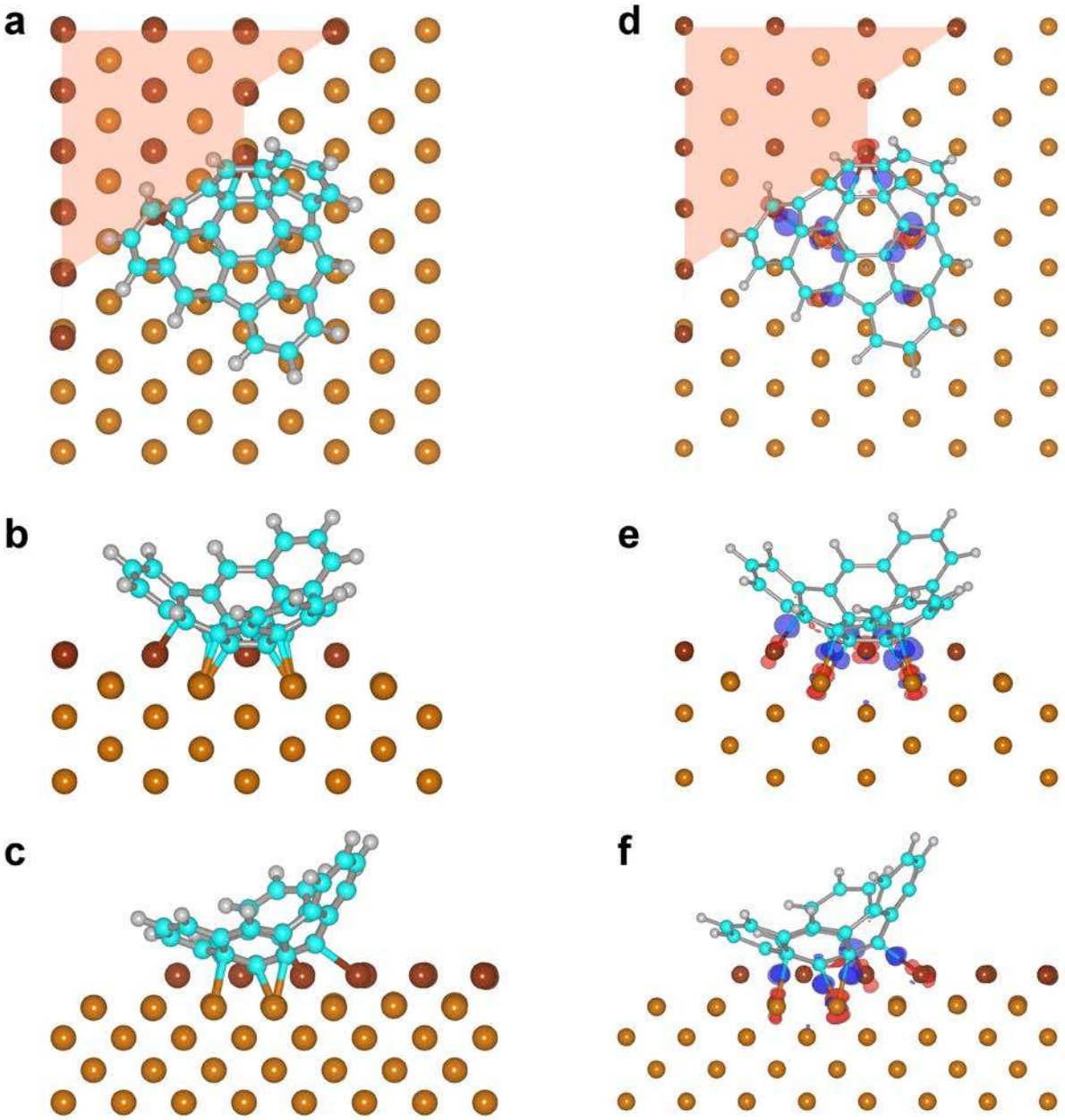

Figure 4 | Single *M*-hemifullerene *(R)*-kink complex. Top (**a**), front (**b**) and side (**c**) views of *M*- hemifullerene bound to an *R*-kink as obtained by DFT calculations. Cu atoms of lower terrace appear light brown, Cu atoms at upper terrace appear dark brown. The bonds are identified via charge density distribution calculations (**d**-**f**). Charge depletion is marked in red, charge accumulation in blue with a contour value of 0.06 e/Å^3. Chirality transfer from the molecule to the metal arises via three η^2– and three η^1–coordinative bonds to Cu atoms

of the metal substrate. One of each type of bond goes to kink atoms, the others to atoms located in the lower terrace.